Segment 2D and 3D Filaments by Learning Structured and Contextual Features

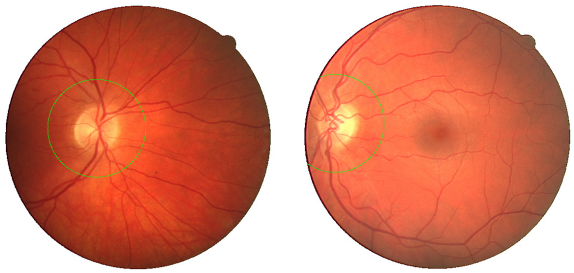

Fig. 1: Exemplar optical disk region masks used during the evaluation on the optical disk region. (Left): The mask is completely inside the fundus mask. (Right): The mask is partially inside the fundus mask, then the intersected area is selected.

I. Exemplar Optical Disk Region Masks

Fig. 1 illustrates two examples of the optical disk region masks used during the evaluation on the optical disk region. Here a masked area is centered around the optical disk with a radius of 100 pixels is applied to extract the region of interest,

II. An Alternative Evaluation Metric in 3D Experiments

On 3D datasets, instead of the evaluation metric that has been described in the main text, where the near boundary voxels are simply ignored, here a slightly different metric is utilized. Basically these near boundary voxels are now still considered but with a weight linear w.r.t. its shortest distance from the ground-truth (a voxel inside the ground-truth is considered as $d_{gt} = 0$). In other words, we assign each voxel a weight w according to its shortest distance d_{gt} to the ground-truth as

$$w = \begin{cases} (d_{gt})/\sigma & \text{if } 0 < d_{gt} < \sigma \\ 1 & \text{otherwise} \end{cases}$$

As shown in Fig. 2, the voxels closer to the ground-truth surface have less influence on evaluation due to the inaccurate in this region. The parameter $\sigma = 2$ is fixed throughout the experiments.

Under this alternative metric, we get the results on the Gold166 which are reported in TABLE I. When comparing with the counterpart (Table III) in the main text, it is clear that the order of all the competing methods remains the same. This suggests that either ignoring the boundary voxles or add small weights would not change the final evaluation results. In this paper we thus stick to the first metric.

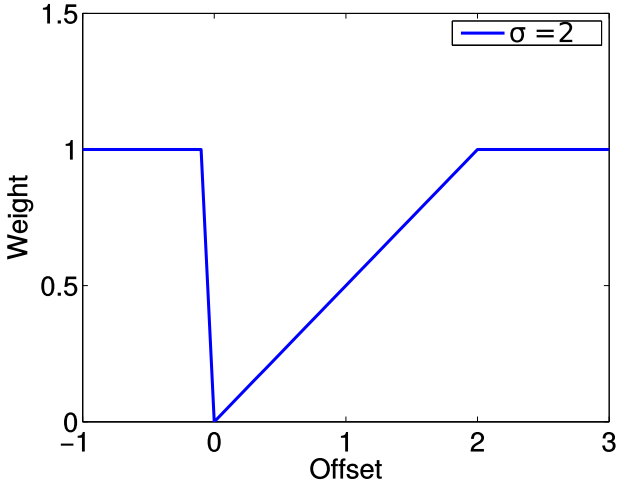

Fig. 2: The weight w with respect to the d_{gt} when $\sigma = 2$

References

[1] D. Martin, C. Fowlkes, D. Tal, and J. Malik, "A database of human segmented natural images and its application to evaluating segmentation algorithms and measuring ecological statistics," in *ICCV*, vol. 2, 2001, pp. 416–423.

[2] V. Mnih and G. E. Hinton, "Learning to label aerial images from noisy data," in *Proceedings of the 29th International Conference on Machine Learning (ICML-12)*, J. Langford and J. Pineau, Eds. New York, NY, USA: ACM, 2012, pp. 567–574.

[3] A. Sironi, E. Turetken, V. Lepetit, and P. Fua, "Multiscale centerline detection," in *IEEE Trans. PAMI*, 2016.

[4] Z. Zhou, S. Sorensen, H. Zeng, M. Hawrylycz, and H. Peng, "Adaptive image enhancement for tracing 3D morphologies of neurons and brain vasculatures," *Neuroinformatics*, vol. 13, no. 2, pp. 153–166, 2015.

[5] H. Xiao and H. Peng, "APP2: automatic tracing of 3D neuron morphology based on hierarchical pruning of a gray-weighted image distance-tree," *Bioinformatics*, vol. 29, no. 11, pp. 1448–54, 2013.

TABLE I: Comparison of 3D neuronal segmentation methods on Gold166 dataset using F1 measure (%) with tolerance $\sigma = 2$.

SF	SF + context distance	Adaptive Enhancement [4]	GWDT [5]	Regression Tubularity [3]
86.22 ± 7.96	**86.60** ± 8.46	70.21 ± 13.80	82.49 ± 9.82	79.64 ± 10.70

TABLE II: Performance statistics of 2D segmentation using F1 measure (%), Precision (%), Recall (%), Specificity (%) and MCC.

		Method										
		SF	**SF + context distance**	**Kernel Boost [?]**	**OOF [?]**	**IUWT [?]**	**Eigen [?]**	**T2T [?]**	**SE [?]**	**B-COSFIRE [?]**	**CNN [?]**	**FC-CRF [?]**
DRIVE	F1 measure	77.57 ± 2.16	78.86 ± 2.15	74.79 ± 2.67	67.01 ± 3.12	68.81 ± 3.31	65.74 ± 4.85	40.56 ± 2.26	60.98 ± 2.75	78.73 ± 1.95	80.07 ± 1.77	78.57 ± 2.08
	Precision	79.31 ± 2.16	80.50 ± 2.15	71.65 ± 2.67	65.76 ± 3.12	69.23 ± 3.31	67.43 ± 4.85	42.72 ± 2.26	55.33 ± 2.75	78.87 ± 1.95	82.03 ± 1.77	78.54 ± 2.08
	Recall	75.95 ± 2.16	77.33 ± 2.15	78.30 ± 2.67	68.42 ± 3.12	68.57 ± 3.31	64.82 ± 4.85	38.80 ± 2.26	68.23 ± 2.75	78.67 ± 1.95	78.23 ± 1.77	78.97 ± 2.08
	Specificity	97.11 ± 2.16	97.28 ± 2.15	95.50 ± 2.67	94.81 ± 3.12	95.57 ± 3.31	95.43 ± 4.85	92.31 ± 2.26	91.95 ± 2.75	96.93 ± 1.95	97.51 ± 1.77	96.84 ± 2.08
	MCC	0.7442 ± 0.0216	0.7589 ± 0.0215	0.7106 ± 0.0267	0.6214 ± 0.0312	0.6436 ± 0.0331	0.6116 ± 0.0485	0.3244 ± 0.0226	0.5511 ± 0.0275	0.7567 ± 0.0195	0.7728 ± 0.0177	0.7556 ± 0.0208